SCIENCE CHINA
Earth Sciences

SPECIAL TOPIC: Remote Sensing and Global Change
• RESEARCH PAPER •

October 2014 Vol.57 No.10: 2317–2329
doi: 10.1007/s11430-014-4919-z

A multi-resolution global land cover dataset through multisource data aggregation

YU Le[1], WANG Jie[2], LI XueCao[1], LI CongCong[3], ZHAO YuanYuan[1] & GONG Peng[1,2,4*]

[1] *Ministry of Education Key Laboratory for Earth System Modeling, Center for Earth System Science, Tsinghua University, Beijing 100084, China;*
[2] *State Key Laboratory of Remote Sensing Science, Institute of Remote Sensing and Digital Earth, Chinese Academy of Sciences, Beijing 100101, China;*
[3] *State Key Laboratory of Remote Sensing Science, and College of Global Change and Earth System Science, Beijing Normal University, Beijing 100875, China;*
[4] *Joint Center for Global Change Studies, Beijing 100875, China*

Received December 13, 2013; accepted April 28, 2014; published online June 27, 2014

Recent developments of 30 m global land characterization datasets (e.g., land cover, vegetation continues field) represent the finest spatial resolution inputs for global scale studies. Here, we present results from further improvement to land cover mapping and impact analysis of spatial resolution on area estimation for different land cover types. We proposed a set of methods to aggregate two existing 30 m resolution circa 2010 global land cover maps, namely FROM-GLC (Finer Resolution Observation and Monitoring-Global Land Cover) and FROM-GLC-seg (Segmentation), with two coarser resolution global maps on development, i.e., Nighttime Light Impervious Surface Area (NL-ISA) and MODIS urban extent (MODIS-urban), to produce an improved 30 m global land cover map—FROM-GLC-agg (Aggregation). It was post-processed using additional coarse resolution datasets (i.e., MCD12Q1, GlobCover2009, MOD44W etc.) to reduce land cover type confusion. Around 98.9% pixels remain 30 m resolution after some post-processing to this dataset. Based on this map, majority aggregation and proportion aggregation approaches were employed to create a multi-resolution hierarchy (i.e., 250 m, 500 m, 1 km, 5 km, 10 km, 25 km, 50 km, 100 km) of land cover maps to meet requirements for different resolutions from different applications. Through accuracy assessment, we found that the best overall accuracies for the post-processed base map (at 30 m) and the three maps subsequently aggregated at 250 m, 500 m, 1 km resolutions are 69.50%, 76.65%, 74.65%, and 73.47%, respectively. Our analysis of area-estimation biases for different land cover types at different resolutions suggests that maps at coarser than 5 km resolution contain at least 5% area estimation error for most land cover types. Proportion layers, which contain precise information on land cover percentage, are suggested for use when coarser resolution land cover data are required.

spatial aggregation, Landsat, MODIS, biodiversity, climate change, multi-resolution, majority vote

Citation: Yu L, Wang J, Li X C, et al. 2014. A multi-resolution global land cover dataset through multisource data aggregation. Science China: Earth Sciences, 57: 2317−2329, doi: 10.1007/s11430-014-4919-z

Since the 1980s, global land cover maps were compiled at 1° and 0.5° spatial resolutions for climate modeling and carbon cycling studies (Matthews, 1983; Olson et al., 1982; Wilson et al., 1985). Earth system modeling, however, requires finer resolution, more frequent, and more precise thematic contents and stable land cover data (Bontemps et al., 2012). Therefore, data from sensor systems such as the Advanced Very High Resolution Radiometer (AVHRR), the MODerate Resolution Imaging Spectroradiometer (MODIS), SPOT-VEGETATION (SPOT-VET), and the MEdium Resolution Imaging Spectrometer (MERIS) have been used

*Corresponding author (email: penggong@tsinghua.edu.cn)

for global land cover mapping using their frequent coverage of the earth surface (e.g., DeFries et al, 1994; Loveland et al., 2000; Hansen et al., 2000; Friedl et al., 2010; Bartholome et al., 2005; Arino et al., 2008, Bontemps et al., 2010; Tateishi et al., 2011). However, the low spatial resolutions of these sensors (250 m/500 m/1 km for MODIS, 1 km for AVHRR and SPOT-VEG, 300 m for MERIS) limited the capability of exploring finer scale land cover types. Thanks to the free availability of Landsat archive, global land cover mapping at medium resolution became possible. Since 2013, global land cover mapping and characterization at 30 m resolution using Landsat Thematic Mapper/Enhanced Thematic Mapper Plus (TM/ETM+) (e.g., Gong et al., 2013; Yu et al., 2013a; 2013b; Sexton et al., 2013; Hansen et al., 2013) have begun to provide more detailed land information to a broad application community.

Finer Resolution Observation and Monitoring-Global Land Cover (FROM-GLC) (Gong et al., 2013) and FROM-GLC-seg (Yu et al., 2013a) are the only two existing global land cover maps at 30 m resolution. However, both of them have limitations. FROM-GLC was produced based on single-date (nominal year 2010) Landsat TM/ETM+ images. Due to the trade-off between temporal frequency and spatial resolution in FROM-GLC, accuracies for land cover types relying on information of phenological dynamics such as agriculture and grasslands are limited. FROM-GLC-seg complemented Landsat TM/ETM+ with 250 m spatial resolution time series MODIS Enhanced Vegetation Index (EVI), bioclimatic variables, digital elevation model (DEM) and soil-water variables using a segmentation approach. The overall accuracy (OA) and accuracies for most land cover types were improved in FROM-GLC-seg, but land cover types in small patches (i.e., water, ice/snow) were underestimated due to the inclusion of coarser-resolution input features. Combining (aggregating) different maps to provide an improved land cover/land use dataset has been adopted in many previous studies (e.g., Sterling et al., 2008; Verburg et al., 2011). This approach considers each pixel from different candidate maps based on decision rules, e.g., fuzzy agreement scoring (Jung et al., 2006), expert knowledge, and regional maps (Fritz et al., 2011; Vancutsem et al., 2013). The potential of accuracy improvement after integrating FROM-GLC and FROM-GLC-seg remains to be evaluated.

Users of global land cover maps also have concerns on the accuracy of spatial resolution, in addition to the accuracies of land cover types. The available land cover data rarely fit perfectly the spatial resolution requirement from specific applications (Quattrochi et al., 1997; Raj et al., 2013). Thus, additional spatial resampling is usually required at the pre-processing stage. According to a survey (Bontemps et al., 2012) to the climate user community, the most frequently used land cover maps in global climate modeling are kilometer level products, such as International Geosphere-Biosphere Programme (IGBP) and Global Land Cover Characterization (GLCC) (Loveland et al., 2000), MODIS land cover (Friedl et al., 2010), GLC2000 (Global Land Cover 2000) (Bartholome et al., 2005) etc. All those datasets are at 1 km or 500 m resolution. However, applications from agriculture, water resources management, and urban planning need finer resolution land cover maps (Yu et al., 2013b; Zhong et al., 2012, 2014; Wang et al., 2012). Studies on public health, biodiversity, wildlife conservation, carbon science, hydrology, and landscape change at large spatial extents also need finer resolutions (i.e., Liang et al., 2010; Mauser et al., 1998; Zhao et al., 2010; Gong et al., 2012). Land cover change data with spatial resolutions coarser than 1 km have been found introducing significant biases in the estimation of terrestrial carbon sequestration, its interannual variability, and spatial pattern (Zhao et al., 2010). Spatial upscaling (reducing resolution) or downscaling (increasing resolution) is a strategy often used to rescale the data before use (i.e., Wilby et al., 1997; Hijmans et al., 2005; Kitron et al., 2006; Ramirez-Villegas et al., 2010). Evaluations at local scale indicate that classification errors or percentage estimation biases of different land cover types are affected differently at different resolutions with scaling (i.e., Moody et al., 1995; Gupta et al. 2000; He et al., 2002; Gardner et al. 2008; Raj et al., 2013). However, there is no similar analysis for land cover map at the global scale.

To support feasible use of global land cover maps in different applications, this paper addresses both map quality improvement and multi-resolution issues. There were two objectives of this study. First, we attempted to assess the potential of combining the strengths of the two existing 30 m land cover maps and overcoming their common weaknesses over impervious areas by combining two coarser resolution impervious maps using a rule-based decision tree technique. Second, post-processing and spatial up-scaling were applied to generate consistent land cover maps in 9 spatial resolution levels (i.e., 30 m, 250 m, 500 m, 1 km, 5 km, 10 km, 25 km, 50 km, 100 km). Area estimation biases for global land cover maps at different resolutions were evaluated quantitatively for the first time.

1 Methods for improving 30 m global land cover mapping

FROM-GLC is a 30 m spatial resolution global land cover map using a total of 8903 Landsat TM/ETM+ scenes (covering the whole globe except Antarctica and Greenland) for a nominal year of 2010 (approximately 3 quarters of the images were from circa 2010 and 1 quarter was from circa 2000) (Gong et al., 2013). A unique classification system (Table 1) focused on land cover types was used in FROM-GLC. Globally, 91433 training samples and 38664 test samples were collected through human interpretation of Landsat images, with reference to MODIS time series, high resolution images and field photos found in Google Earth

Table 1 Classification system for FROM-GLC (modified from Gong et al., 2013)

Level 1	Level 2	Level 1	Level 2
Croplands	Paddy-rice	Water	Terrestrial water
	Greenhouse		Sea
	Other-crop	Impervious	High-albedo
Forests	Broadleaf		Low-albedo
	Needleleaf	Barelands	Alkali-soils
	Mixed		Sand
	Orchard		Rock
Grasslands	Managed		Crop-bare
	Nature		River-bed
	Wetland-grass		Other-bare
	Tundra-grass	Snow/ice	Snow
Shrublands	Shrublands		Ice
	Tundra-Shrub	Cloud	

(taken from Panoramio, http://www.panoramio.com/). Four supervised classifiers, i.e., Maximum Likelihood Classifier (MLC), J48 Decision Tree, Support vector machine (SVM), and Random Forest (RF) were used to produce four land cover maps, among which SVM has the best OA (Level 1 OA = 63.69%, hereinafter OA referred to as Level 1 OA).

FROM-GLC-seg is an amended version of FROM-GLC (Yu et al., 2013a). A segmentation approach was used in FROM-GLC-seg to integrate multi-resolution datasets, including Landsat TM/ETM+ (30 m), MODIS EVI time series (250 m), bioclimatic variables (1 km), global DEM (1 km), and soil-water variables (1 km). FROM-GLC-seg used the same training/test samples as FROM-GLC, and followed the same classification system with a slight modification. Impervious land cover type was not mapped, due to severe spectral mixing effects in coarser resolution images. In addition, clouds, which temporally existed in Landsat TM/ETM+ images, were removed as well. The RF classifier was used and achieved a better OA (OA=64.42%).

In both FROM-GLC and FROM-GLC-seg, less emphasis was given to the impervious cover type as it shall be mapped with different methods (Wang et al., 2010; 2012; Gong and Howarth, 1990; 1992a; 1992b). One of the primary obstacles to urban land cover mapping using remote sensing is the diversity and spectral heterogeneity of urban reflectance (Small, 2005). Mapping impervious surface cover is important because it reflects land-use patterns related to socio-economic activities and environmental/ ecological impacts (e.g., Jensen et al., 1999; Small, 2005). Thus several global impervious (including urban) maps were produced, and most of them were generated using single type mapping approaches.

In this paper, we improved the 30 m land cover product from two aspects: (1) Downscaling the best two impervious products—Nighttime Light Impervious Surface Area (NL-ISA) (Elvidge et al., 2007) and MODIS urban extent (MODIS-urban) (Schneider et al., 2009; 2010) to 30 m spatial resolution; and (2) building a decision tree to aggregate those two impervious products with FROM-GLC and FROM-GLC-seg.

1.1 Impervious type downscaling

Elvidge et al. (2007) produced a 1km global impervious surface area (ISA) density map using the radiance calibrated nighttime lights (http://www.ngdc.noaa.gov/dmsp/downloadV4composites.html) and the Landscan population count (http://www.ornl.gov/sci/landscan/) with reference to the 30 m USGS Landsat derived ISA (from the NLCD-2001) (http://www.epa.gov/mrlc/nlcd-2001.html). This product was evaluated by comparing with USGS ISA for conterminous US (7.4% less than USGS ISA.).

In order to make the NL-ISA serve the purpose of global land cover mapping, an optimal threshold is needed to decide a pixel as impervious or not globally. We stepped through percent cover of ISA from 1 to100 (% impervious coverage in a pixel) and calculated the OA for classifying impervious area samples and barelands samples (which is the most seriously confused type with impervious area, see Gong et al., 2013) extracted from global land cover sample sets developed in Gong et al. (2013). The best OA (99.57%) was reached when the percent value is 4 (4%), which was chosen as the threshold of impervious and non-impervious in this study (Figure 1). Even with such a low threshold value, many urban areas were still missed out. Then we used a global urban product MODIS-urban to reclaim impervious areas missing from thresholding the NL-ISA.

Schneider et al. (2009, 2010) produced 500 m global urban extent map (for the years 2000–2001) using MODIS data based on a supervised decision tree classification algorithm using a global training database. To overcome confusions between urban and built-up lands and other land cover

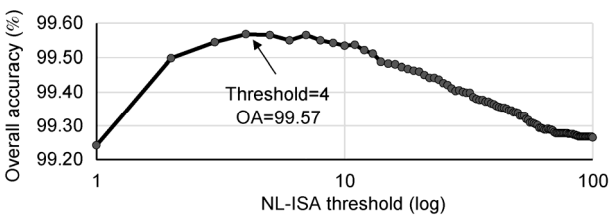

Figure 1 Accuracy of classifying impervious and barelands samples under different NL-ISA thresholds.

types, a stratification based on climate, vegetation, and urban topology was developed that allowed region-specific processing. This product has an OA of 93% when evaluated using stratified random samples from 140 cities in the world. Compared to NL-ISA, MODIS-urban performed better (precisely and correctly) in urban areas especially when the urban size is small. Figure 2 shows the missed proportion of urban areas in MODIS-urban when different thresholds of NL-ISA are used. A threshold value of 4 missed 24.71% urban areas.

Both NL-ISA and MODIS-urban product were included to improve the impervious land cover type in 30 m global land cover maps using a spatial downscaling approach (Figure 3). In this process, any impervious pixel indicated in NL-ISA or MODIS-urban was taken as impervious to guide FROM-GLC and FROM-GLC-seg. Compared with the Landsat TM/ETM+ images, the impervious area in the aggregation map (namely FROM-GLC-agg) is more reasonable than FROM-GLC.

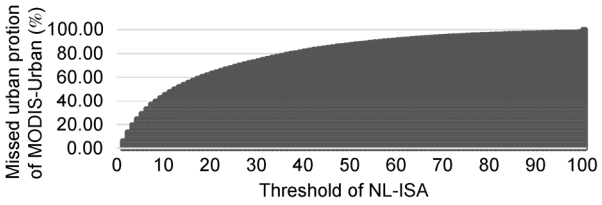

Figure 2 Missing urban proportion of MODIS-Urban product under different NL-ISA thresholds.

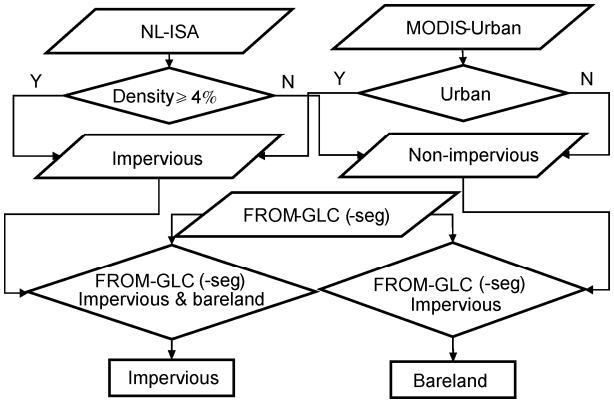

Figure 3 Workflow of impervious cover aggregation.

1.2 Aggregating 30 m land cover maps

As mentioned above, both FROM-GLC and FROM-GLC-seg have merits: FROM-GLC-seg has better accuracies for vegetation types and barelands, but land cover types that occur in small patches (e.g., river streams, snow/ice) were mapped better in FROM-GLC (which is purely 30 m for each pixel). A new 30 m global land cover product (FROM-GLC-agg) was generated according to an aggregation procedure shown in Figure 4. In this process, pixels classified as vegetation land cover types (i.e., croplands, forests, shrublands, and grasslands) and barelands are all taken from FROM-GLC-seg. Water bodies and snow/ice types in FROM-GLC-seg are smoother with much less pepper and salt noise, but the drawback is that small streams are neglected (Yu et al., 2013a). To obtain those small sized water bodies, water and snow/ice in FROM-GLC are added to the FROM-GLC-seg map. In order to reduce the misclassification below heavy cloud (no underneath information can be captured), we left cloud as a land cover type (also as a quality flag).

Following the workflow introduced above, a new global 30 m land cover map—FROM-GLC-agg was created (Figure 5). The map accuracy was validated by 38664 globally distributed test samples (Gong et al., 2013; Zhao et al., in review). The confusion matrix (Table 2) indicates an OA of 65.51% for FROM-GLC-agg, which is better than FROM-GLC (63.69%) and FROM-GLC-seg (64.42%).

The distribution of wrongly classified sample locations was aggregated to WWF ecoregion unit (867 geographical units in total) (Olson et al., 2001), which represents biogeographically homogeneous areas (Figure 6). It shows that errors are distributed along transitional zones. On the contrary, rainforest, dry desert, and water bodies are the regions relatively easier to classify.

2 Multi-resolution land cover maps

We generated multi-resolution global land cover products from FROM-GLC-agg to serve the requirements of different spatial resolution needs by different applications. However, issues in FROM-GLC-agg are still obvious with confusions in land cover types (Table 1, Figure 6). Known

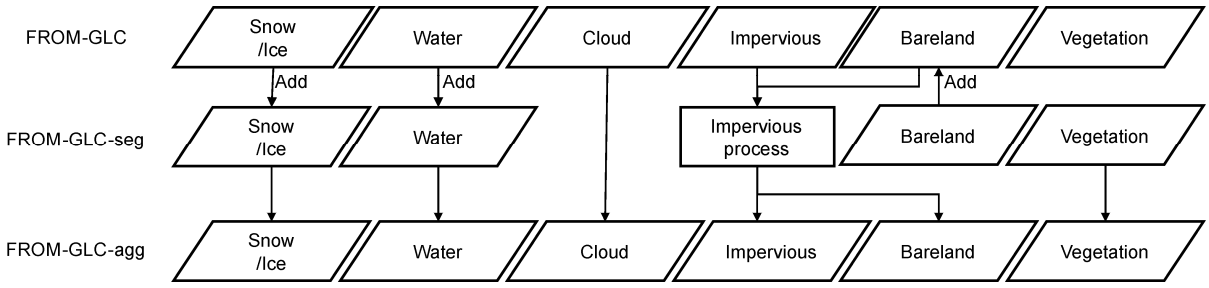

Figure 4 Workflow of FROM-GLC-agg.

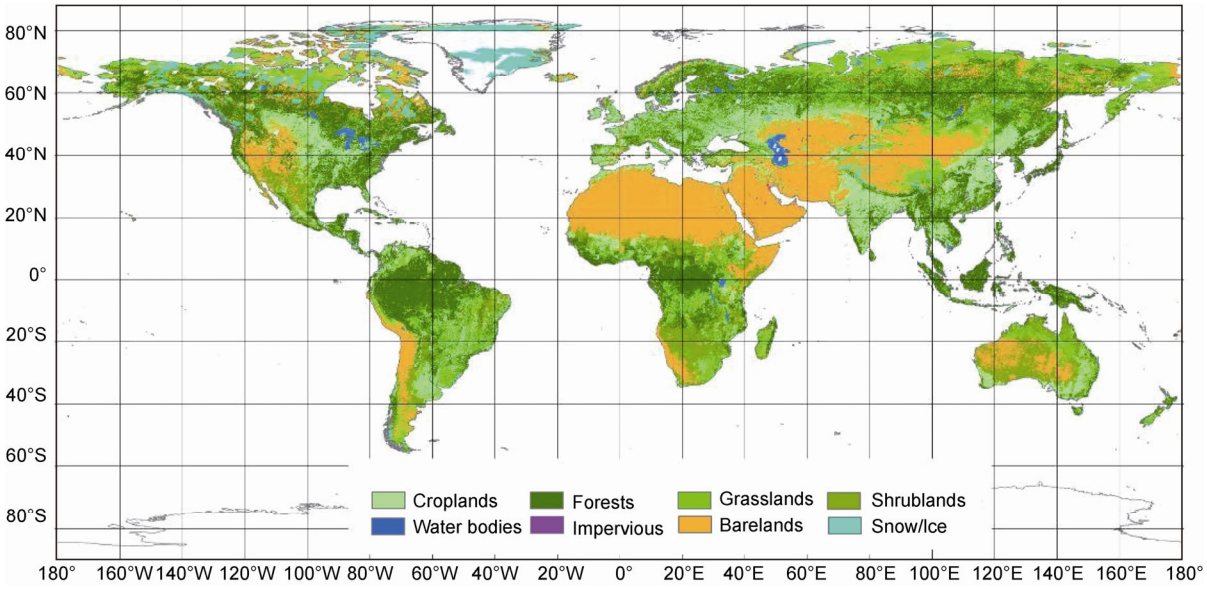

Figure 5 A new global aggregated map - FROM-GLC-agg.

Table 2 Confusion table for the FROM-GLC-agg[a)]

	1	2	3	4	5	6	7	8	9	PA (%)
Croplands (1)	**2587**	388	400	182	43	21	248	0	14	66.62
Forests (2)	445	**8982**	792	645	163	8	202	2	122	79.06
Grasslands (3)	970	1114	**2522**	711	111	13	1843	0	44	34.42
Shrublands (4)	266	600	823	**1682**	51	8	988	1	16	37.93
Water bodies (5)	13	15	19	2	**1336**	5	32	5	8	93.10
Impervious (6)	89	49	35	15	4	**69**	11	0	4	25.00
Barelands (7)	105	17	122	242	57	42	**5688**	0	5	90.60
Snow/Ice (8)	2	16	26	2	150	0	69	**430**	39	58.58
Clouds (9)	14	37	7	1	7	4	30	1	**511**	83.50
UA (%)	57.60	80.07	53.14	48.31	69.51	40.59	62.43	97.95	66.97	**65.51**

a) PA: Producer's Accuracy, UA: User's Accuracy.

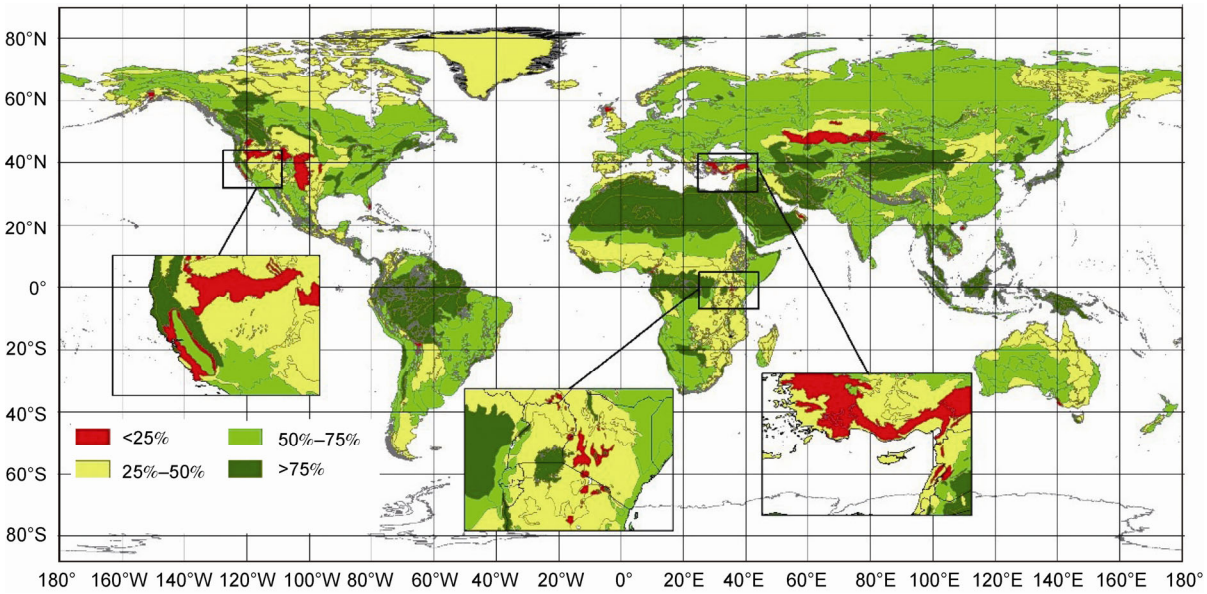

Figure 6 Distribution of proportion of correctly classified test samples in each ecoregion unit.

issues include: (1) There are about 0.65 million km^2 of terrestrial land areas (excluding Antarctica and Greenland) not covered (indicated as "No data" in FROM-GLC-agg) by Landsat TM/ETM+ images. These areas were distributed mostly within the Arctic region. (2) Cloud covers were mapped as a land cover type (as a quality flag, covering about 0.97 Million km^2) in FROM-GLC-agg. Therefore, the underneath types were not available. (3) Shadows from clouds and mountains were mixed with water due to similar low spectral reflectance. (4) Overestimation of barelands is common due to lack of time-series Landsat TM/ETM+ images in producing FROM-GLC-agg. Thus, temporal barelands tended to be misclassified. For example, steppes in some cold regions (e.g., Tibet Plateau) were wrongly classified as barelands. Also for images with heavy clouds mixed with water (mostly on ocean/terrestrial boundaries), clouds can be misclassified as barelands as well.

Mitigating such misclassifications in FROM-GLC-agg, we used land cover information from coarser resolution data sources (Figure 7). Additional datasets were integrated to improve FROM-GLC-agg based on a quality criterion, i.e., any high quality (accuracy) data would supersede the low quality data (pixels). Drawbacks mentioned above were handled as follows: (1) No data pixels and cloud pixels were replaced primarily by MODIS land cover product (Friedl et al., 2010) with a small proportion by GlobCover2009 (Bontemps et al., 2010). Both products were crosswalked to FROM-GLC using a supplementary Table S1(http: link. springer.com). (2) Confusions between water bodies and shadows were processed using MODIS land cover, GlobCover2009, global water mask (Carroll et al., 2004). (3) Bareland overestimation was reduced by using a MODIS-based land cover map using spatial temporal consistency check (Land Cover map with Spatial Temporal Consistency check, LC-STC) (Wang et al., 2014). (4) Land cover type confusions in ocean areas were filtered using a shoreline database GSHHG (Global Self- consistent, Hierarchical, High-resolution Geography Database) (Wessel et al., 1996). Note that the spatial resolution of those replaced pixels is no longer 30 m (equal to or coarser than 250 m in fact). However, only around 1.09% of land area pixels have been replaced by coarser resolution data. The remaining 98.9% pixels are still at 30 meter resolution. Thus, we still call this post-processed map a 30 m "base map", which is the beginning of multi-resolution processing. This process resulted in the multi-resolution land cover maps–FROM-GLC-hierarchy.

FROM-GLC-hierarchy was produced using category upscaling approach (category spatial aggregation), in which class type is assigned to a pixel at coarse resolution based on the class types at finer resolution. Many upscaling approaches have been developed, including the majority rule-based upscaling (Turner et al. 1989a, 1989b; Moody et al., 1994, 1995; He et al., 2002; Raj et al., 2013), random rule-based upscaling (He et al., 2002), and point-centered distance-weighted moving window upscaling (Gardner et al., 2008) etc. Previous studies on data bias effects across scales were based on small study areas (local scale) or simulated data (Woodcock et al. 1987; Turner et al. 1989a; Moody et al., 1995; He et al., 2002; Raj et al., 2013). Area statistics of land cover are bound to be biased after aggregation. General consensus includes (He et al., 2002): the rates of over/under-estimation are linked to spatial pattern of different land cover types. For example, dominant types get overestimated and land cover types with smaller patches are

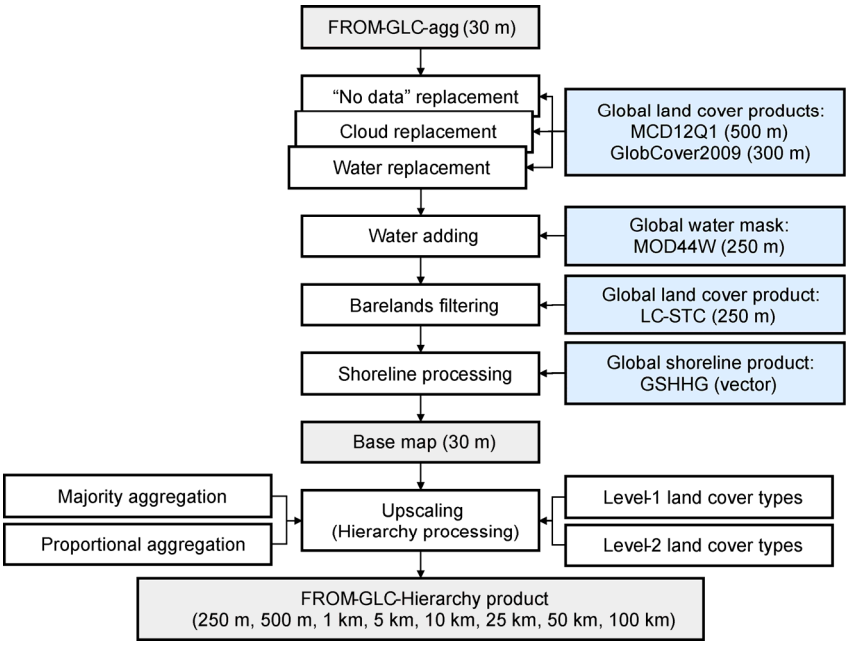

Figure 7 Workflow of FROM-GLC-Hierarchy.

underestimated.

For the first time, scale-related land cover area bias was quantitatively analyzed globally. In this study, we used a majority aggregation as an example to examine the upscaling impact of area estimation biases at different levels on different land cover types using global land cover maps. Majority rule-based aggregation selects the most frequently occurring type from the pixels under consideration (Figure 8(a)). When there is more than one major type, the dominant type is selected randomly. A way (proportion aggregation) for keeping the proportion of different land cover types at different resolution was also used in this study to provide unbiased coarse resolution products. In this way, for each pixel, the proportions of all land cover types were recorded by creating multiple layers, each of which represents a different land cover type (each pixel in different resolution layers indicates the percentage of certain land cover types in the base map) (Figure 8(b)). Eight coarser resolution (i.e., 250 m, 500 m, 1 km, 5 km, 10 km, 25 km, 50 km, and 100 km) land cover products were generated by using these two aggregation approaches.

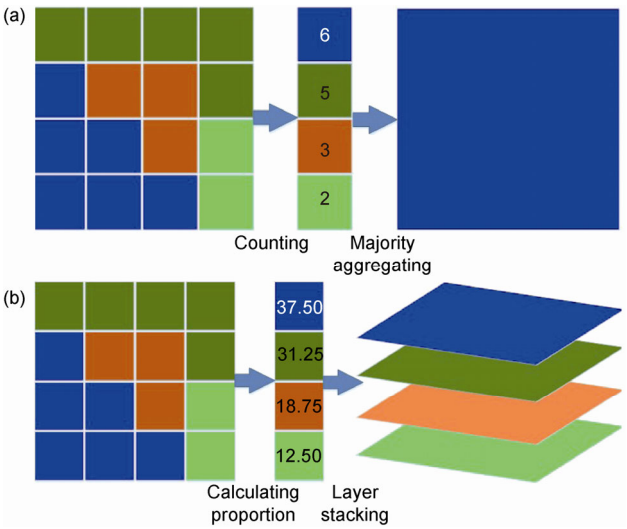

Figure 8 Illustration of majority aggregation (a) and proportion aggregation (b).

Figure 9 and Figure 10 show the result after post-processing and majority aggregation respectively for a location (1200 km × 1200 km, including Northern China Plain) with the boundary of a MODIS Tile H27V05. "No Data" (pixels in black color in Figure 9(a)) and cloud type (pixels in white color in Figure 9(a)) were replaced by new land cover types (Figure 9(b)). Overestimated water bodies (located in southwest in Figure 9(a)) and barelands (located in northeast in Figure 9(a)) were corrected (Figure 9(b)).

Results after majority aggregation to 250 m–100 km are shown in Figure 10. For this region, croplands, forests, and water bodies are the dominant land cover types. Those types are overestimated when resolutions go coarser, but impervious area disappeared after the resolution goes beyond 50 km.

Accuracies of those maps were evaluated by the same set of 38664 test samples. The post-processing for a base map improved the OA to 67.63%, which is 2.12% better than FROM-GLC-agg (65.51%). In addition, a subset (16105) of the test sample (which indicates spatially homogenous pixels at 1km resolution, called "big sample") (Gong et al., 2013) was selected to evaluate coarser resolution maps after the majority aggregation. OAs for global land cover maps at 250m, 500m, and 1km are 74.10%, 71.86%, and 70.77%, respectively. Considering the seasonal uncertainty for a proportion of test samples (which means the land cover type of those samples may change in growing season and outside of growing season), we selected samples without such uncertainty for another accuracy evaluation. In total, 30616

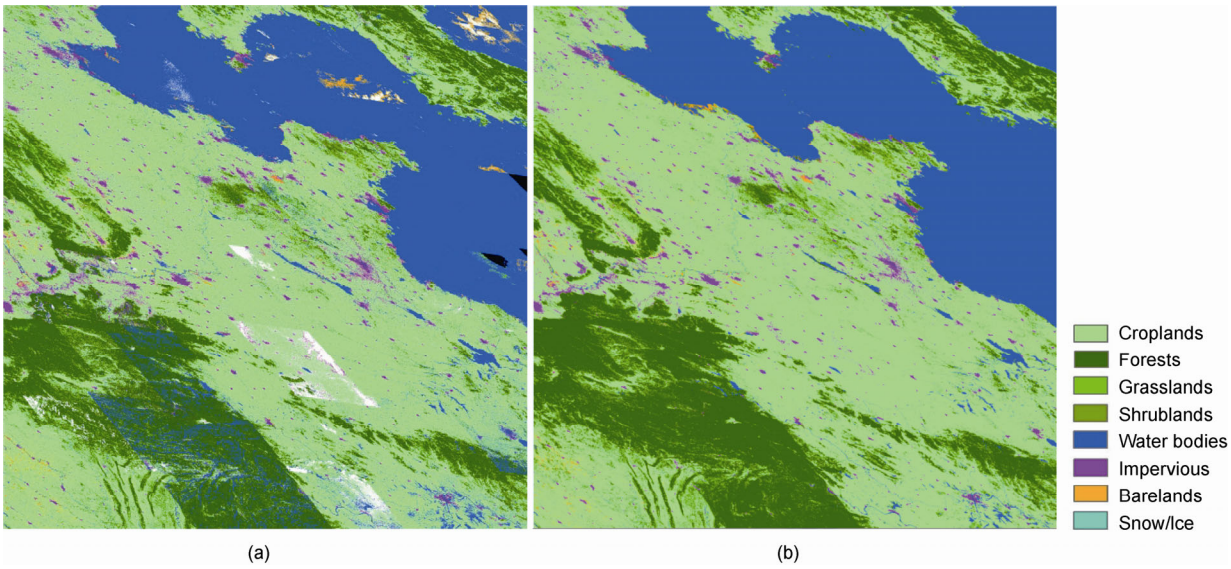

Figure 9 Before (a) and after (b) post-processing (image spatial resolution is 30 m).

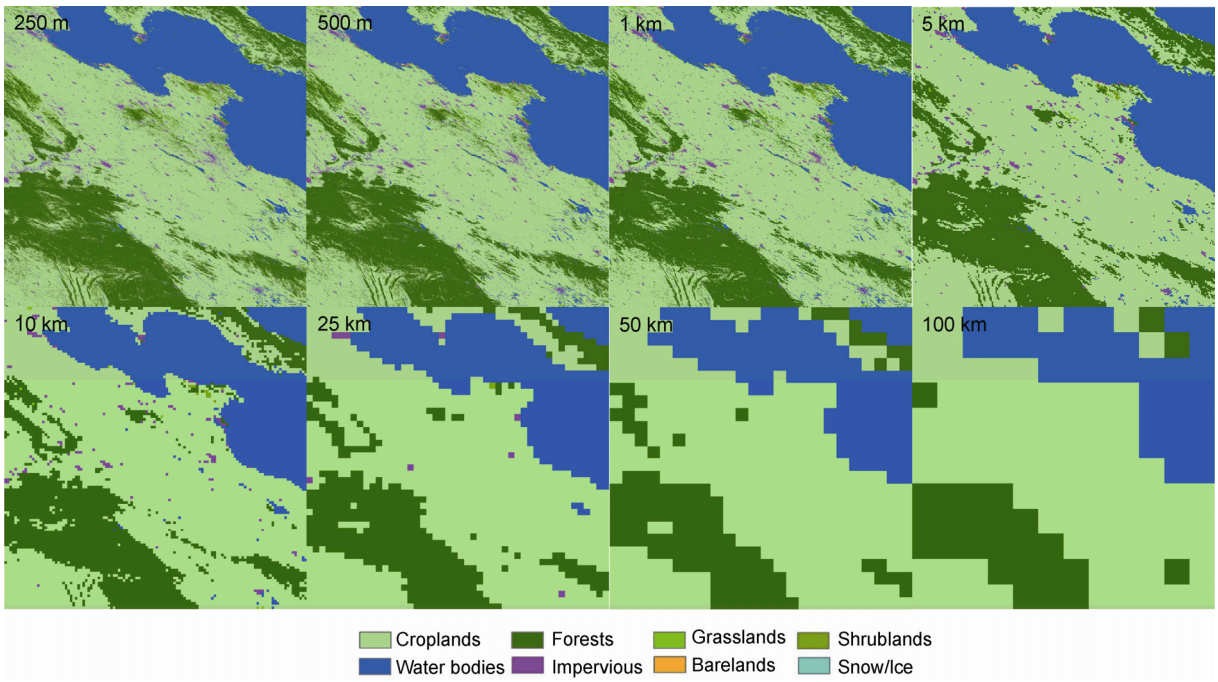

Figure 10 Example of land cover maps after majority aggregation.

sample points were selected; and 13221 of them are big sample units. The OA for the base map is 69.50%, which is evaluated by 30616 samples. OAs for maps at 250 m, 500 m, and 1 km spatial resolution are 76.65%, 74.65%, and 73.47%, respectively, which were evaluated by 13221 big sample units. OAs for maps at coarser resolution (>5 km) were not calculated due to the lack of test samples at corresponding scales. Further accuracy analyses for those maps are found in section 3.3.

3 Discussions

3.1 Comparisons of FROM-GLC, FROM-GLC-seg, and FROM-GLC-agg

From OA, we can see the FROM-GLC-agg (65.51%) is better than FROM-GLC (63.69%) and FROM-GLC-seg (64.42%) directly (Table 3). For a detailed comparison, the classification accuracy was assessed using sample-based confusion matrix and statistical significance test. Many metrics were calculated for this accuracy comparison (Table 3), including: OA, Kappa coefficient (K), Variance of K (K_{var}), Confidence Interval at 95% for K (CI), Producer's Accuracy (PA), and User's Accuracy (UA). A significance test (Z-score) is done to compare each pair of Kappa. If a Z-score is greater than 1.96, then the difference is significant at the 0.95 probability level.

Z-scores among those three products are Z(FROM-GLC-agg, FROM-GLC-seg)=3.7382, Z(FROM-GLC-agg, FROM-GLC)=6.8198, and Z(FROM-GLC-seg, FROM-GLC)=3.0817, indicating that FROM-GLC-agg is significantly better than FROM-GLC-seg and FROM-GLC, and FROM-GLC-seg is significantly better than FROM-GLC.

In terms of UA and PA for individual land cover types, FROM-GLC-agg achieved the best in UA for four land cover types (croplands, impervious, barelands, and snow/ice; the cloud cover type is excluded), and the second best UA for two types (forests and grasslands); it also achieved the best in PA for two land cover types (water bodies and impervious), and the second best in PA for five land cover types (croplands, forests, grasslands, shrublands, and barelands). According to the total sum of best and second best land cover types for all UA, PA, the rank order is FROM-GLC-agg (6 best/second best UA, 7 best/second best PA), FROM-GLC (5 best/second best UA, 5 best/ second best PA), FROM-GLC-seg (3 best/second best UA, 5 best/second best PA).

3.2 Mosaic boundary discontinuity

Different from previous global land cover maps derived from low spatial resolution but high collection frequency, for medium resolution Landsat TM/ETM+ images, it is still difficult to collect data for the entire globe in a consistent season of a year. At the sample selection stage (Landsat TM/ETM+ interpretation) of FROM-GLC, they followed a "what you see is what you get" principle to prevent subjective inference of image information from apparent land cover (Gong et al., 2013). Thus, seasonal variation of images affects the samples and it was finally captured by land cover maps. The follow-up version, FROM-GLC-seg, reduced this mosaic boundary discontinuity appearance by

Table 3 Accuracy comparison between FROM-GLC, FROM-GLC-seg and FROM-GLC-agg

	FROM-GLC		FROM-GLC-seg		FROM-GLC-agg	
OA	63.69%		64.42%		65.51%	
K	0.5429		0.5562		0.5722	
K_{var}	9.2804×10^{-6}		9.2137×10^{-6}		9.1341×10^{-6}	
CI	[0.5370, 0.5489]		[0.5502, 0.5621]		[0.5663, 0.5781]	
	UA (%)	PA (%)	UA (%)	PA (%)	UA (%)	PA (%)
Croplands	43.24	37.59	55.21	67.63	57.60	66.62
Forests	80.16	77.10	79.13	80.09	80.07	79.06
Grasslands	53.66	34.18	52.43	34.57	53.14	34.42
Shrublands	49.11	34.73	48.89	38.45	48.31	37.93
Water Bodies	82.88	88.41	72.02	87.72	69.51	93.10
Impervious	34.88	10.53	-	-	40.59	25.00
Barelands	56.38	93.45	60.64	91.23	62.43	90.60
Snow & Ice	96.54	85.94	80.87	63.35	97.95	58.58
Clouds	65.82	83.63	-	-	66.97	83.50

using multi-temporal MODIS EVI datasets, but in many cases it is still visible. In FROM-GLC-agg, boundaries of map mosaics are still apparently noticeable in Figure 5.

The mosaic appearance reflects the seasonal difference in neighboring Landsat images calculated from MODIS EVI time series in year 2010 (Figure 11). Images used for North America, Europe, Southern Africa, Central Amazon, and Russia are relatively more consistent. Although several visual improvement methods could be used to reduce the mosaic appearance by using information for two well co-registered overlapped areas (e.g., Yu et al., 2012), it is a visual enhancement method and quite time consuming. A better way is to replace Landsat TM/ETM+ scenes collected in improper seasons with more careful data selection based on phenology and scene quality (Franks et al., 2009; Li et al., 2014). One way to improve the visual appearance and accuracies of 30 m global land cover map is to use multi-temporal Landsat TM/ETM+ images. For example, the Landsat image time-series were useful for identifying idle, single-, and multi-cropped fields (Zhong et al., 2012).

To evaluate the potential capability of multi-temporal TM/ETM+, we analyzed the coverage rate (including cloud coverage less than 20% only) on each scene from 1972 since the launch of Landsat-1 (Figure 12). Averagely for each Landsat scene, the whole land area on Earth has been revisited more than 4 times in a year, and the revisit number after 2000 has increased to more than 6 times. A recent analysis of global availability of Landsat TM/ETM+ images also indicates the same capacity (Kovlskyy et al., 2013). It also indicates that the Landsat TM/ETM+ images are an important source for global scale research at fine resolution. Therefore, mining information from such a huge dataset

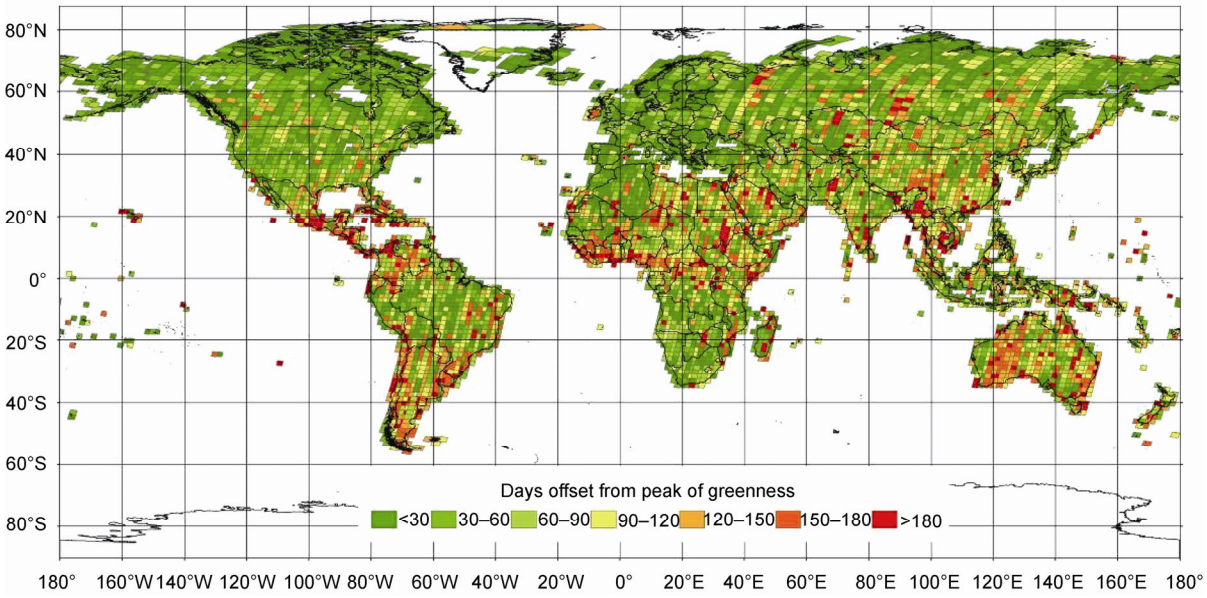

Figure 11 Seasonality difference indicated by the differences between image acquisition dates with top greenness.

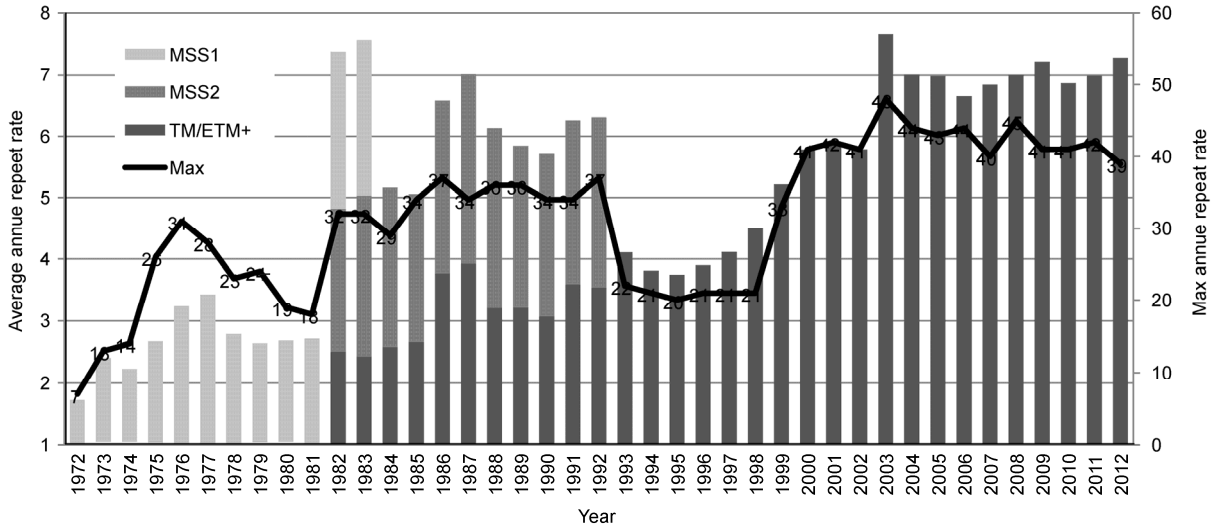

Figure 12 Landsat 1–7 coverage frequency for the same path and row in different years.

efficiently is crucial. Growing demands for high performance computing has emerged in global land cover mapping (Gong et al., 2013; Hansen et al., 2013).

3.3 Area bias analysis at different resolutions

The biases of different land cover types at different resolutions are shown in scatter plots in Figure 13. Each dot in these scatter plots is a MODIS tile (1200 km×1200 km), the *x*-axis is the area proportion for a certain land cover type in the base map, while the *y*-axis is the area proportion at different resolutions after majority aggregation. We can see from these plots that most land cover areas are overestimated (dots distributed above 1∶1 line) at coarser resolutions except for impervious and snow/ice (dots distributed below 1∶1 line). Especially for impervious, distortion in area estimation is considerably large.

Area biases change along the resolution. Take the cropland for example (Table 4), a bias of 1% was produced at 250 m, but it increased to 8% after the resolution dropped to coarser than 25 km. The coefficient of determination R^2 value in linear fitting was decreased from 1 to 0.95. In terms of root mean square error (RMSE) and normalized RMSE (NRMSE), bigger errors were introduced at coarser resolution levels.

A quantitative bias indicates the amount of over- or under-estimation in area for different land cover types at different resolution levels (Table 5). For clarity, biases less

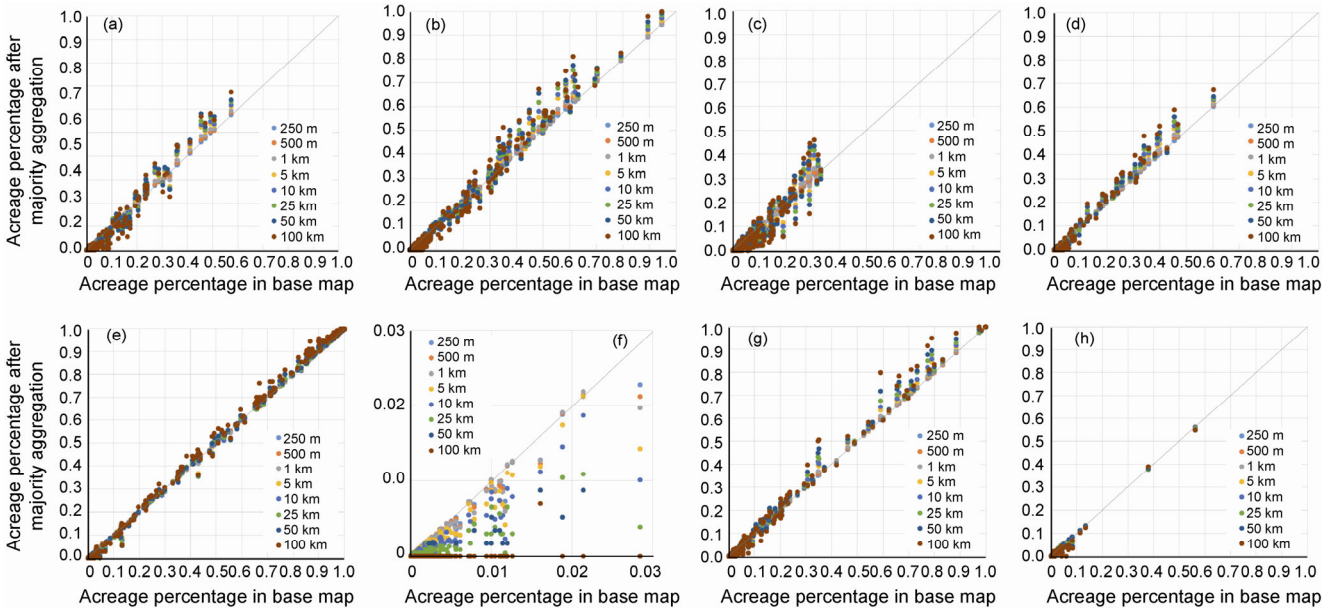

Figure 13 Scatter plots of area proportion of eight land cover types and maps at different resolutions. (a) Croplands; (b) forests; (c) grasslands; (d) shrublands; (e) water bodies; (f) impervious; (g) barelands; (h) snow/ice in base map (30 m).

Table 4 Liner fitting parameters of cropland at different spatial resolution

Resolution	Slope	Offset	R^2	RMSE	NRMSE
250 m	1.01	-3.43×10^{-4}	1.00	1.15×10^{-3}	2.00×10^{-3}
500 m	1.01	-9.44×10^{-4}	9.99×10^{-1}	2.99×10^{-3}	5.20×10^{-3}
1 km	1.03	-1.76×10^{-3}	9.97×10^{-1}	6.03×10^{-3}	1.05×10^{-2}
5 km	1.06	-3.51×10^{-3}	9.88×10^{-1}	1.26×10^{-2}	2.19×10^{-2}
10 km	1.07	-4.25×10^{-3}	9.84×10^{-1}	1.50×10^{-2}	2.61×10^{-2}
25 km	1.08	-5.48×10^{-3}	9.77×10^{-1}	1.82×10^{-2}	3.17×10^{-2}
50 km	1.10	-6.87×10^{-3}	9.68×10^{-1}	2.18×10^{-2}	3.79×10^{-2}
100 km	1.08	-8.29×10^{-3}	9.49×10^{-1}	2.60×10^{-2}	4.52×10^{-2}

Table 5 Area bias caused by majority aggregation for different land cover types at different spatial resolutions [a)]

Resolution	1	2	3	4	5	6	7	8
250 m	0.53%	0.66%	0.39%	0.57%	0.02%	–11.99%	0.10%	–0.12%
500 m	*1.32%*	*1.66%*	0.62%	*1.72%*	–0.04%	–14.10%	0.36%	–0.33%
1 km	*2.97%*	*2.54%*	*1.93%*	*3.25%*	0.03%	–15.07%	0.86%	–0.45%
5 km	**6.09%**	**5.22%**	*3.65%*	**6.20%**	0.41%	–27.79%	*2.12%*	–0.30%
10 km	**7.21%**	**6.45%**	*3.64%*	**7.63%**	0.58%	–41.88%	*2.85%*	–0.61%
25 km	**8.42%**	**8.18%**	*2.96%*	**9.78%**	0.81%	–65.61%	*4.15%*	*–1.90%*
50 km	**9.86%**	**9.87%**	*2.44%*	11.69%	1.00%	–81.31%	*5.39%*	*–2.80%*
100 km	**8.24%**	11.40%	*3.78%*	15.68%	*1.17%*	–96.85%	**7.26%**	*–4.49%*

a) 1, Croplands; 2, forests; 3, grasslands; 4, shrublands; 5, water bodies; 6, impervious; 7, barelands; 8, snow/ice.

than ±1% are underlined, italics for ±1%–3%, bold for ±3%–10%, and others for >±10%. This information can serve as a reference for users to choose land cover datasets at different spatial resolutions. From this table, we may draw a general conclusion: for coarser than 5 km, the majority aggregation introduces greater than 5% bias in area estimation for most land cover types. It is better to use a proportion layer that keeps the original percentage for different land cover types. This analysis also raises a general awareness of land cover area under- or over-estimation when using coarser resolution land cover datasets. These biases can be propagated in application models that use land cover as input.

4 Conclusions

We developed an approach to aggregate FROM-GLC, FROM-GLC-seg to produce a better global land cover map—FROM-GLC-agg. This map has an overall accuracy of 65.51%, which is significantly better than FROM-GLC (63.69%) and FROM-GLC-seg (64.42%). With some additional post-processing to the FROM-GLC-agg, an improved version was used as the 30 m base map to construct the hierarchical dataset (FROM-GLC-Hierarchy, including 9 spatial resolution levels, i.e., 30 m, 250 m, 500 m, 1 km, 5 km, 10 km, 25 km, 50 km, and 100 km). The best OAs for the 30m base map and the aggregated 250m, 500m, and 1km resolution in the FROM-GLC-Hierarchy are 69.50%, 76.65%, 74.65%, and 73.47%, respectively. The framework used in constructing the global land cover hierarchy is open to any type of high quality global/regional land cover data products (e.g., USA's National Land Cover Database (NLCD), China's NLCD, European Corine land cover (CLC)) and single land cover layers (e.g., water mask, vegetation continues fields), wetland map (Zhu et al., 2014) at fine spatial resolutions. According to the area bias experiments with various aggregation levels for different land cover types, land cover products with resolutions coarser than 5 km may lead to large (>5%) over-/under-estimation in area. Therefore, Land cover proportion layers in this hierarchy should be used in applications that require coarser resolution land cover information. The FROM-GLC, FROM-GLC-seg, FROM-GLC-agg, and FROM-GLC-Hierarchy products are all freely available online at http://data.ess.tsinghua.edu.cn.

This work was supported by the National High-tech R&D Program of China (Grant No. 2009AA12200101), the National Natural Science Foundation of China (Grant No. 41301445), an Open Fund from the State Key Laboratory of Remote Sensing Science (Grant No. OFSLRSS201202), and a research grant from Tsinghua University (Grant No. 2012Z02287). We also thank Dr. Mark Broich at the University of New South Wales for valuable discussions on some result analysis in this paper.

Arino O, Bicheron P, Achard F, et al. 2008. GLOBCOVER The most detailed portrait of Earth. ESA Bull-Euro Space Agency, 136: 24–31

Bartholome E, Belward A S. 2005. GLC2000: A new approach to global land cover mapping from Earth observation data. Int J Remote Sens, 26: 1959–1977

Bontemps S, Defourny P, Bogaert E V, et al. 2010. GLOBCOVER2009 Products Description and Validation Report. http://due.esrin.esa.int/globcover/LandCover2009/GLOBCOVER2009_Validation_Report_2.2.pdf

Bontemps S, Herold M, Kooistra L, et al. 2012. Revisiting land cover

observation to address the needs of the climate modeling community. Biogesciences, 9: 2145–2157
Carroll M L, DiMiceli C M, Sohlberg R A, et al. 2004. 250 m MODIS Normalized Difference Vegetation Index, 250ndvi28920033435, Collection 4. Maryland: University of Maryland
DeFries R S, Townshend J R G. 1994. NDVI-derived land cover classification at a global scale. Int J Remote Sens, 15: 3567–3586
Elvidge C D, Tuttle B T, Suttle P C, et al. 2007. Global distribution and density of constructed impervious surfaces. Sensor, 7: 1962–1979
Franks S, Masek J G, Headley R M K, et al. 2009. Large area scene selection interface (LASSI): Methodology of selecting Landsat imagery for the Global Land Survey 2005. Photogramm Eng Remote Sens, 75: 1287–1296
Friedl M A, Sulla-Menashe D, Tan B, et al. 2010. MODIS Collection 5 global land cover: Algorithm refinements and characterization of new datasets. Remote Sens Environ, 114: 168–182
Fritz S, You L, Bun A, et al. 2011. Cropland for sub-Saharan Africa: a synergistic approach using five land cover data sets. Geophys Res Lett, 38: L04404
Gardner R H, Lookingbill T R, Townsend P A, et al. 2008. A New Approach for Rescaling Land Cover Data. Landsc Ecol, 23: 513–526
Gong P, Howarth P J. 1990. The use of structural information for improving land-cover classification accuracies at the rural-urban fringe. Photogramm Eng Remote Sens, 56: 67–73
Gong P, Howarth P J. 1992a. Frequency-based contextual classification and grey-level vector reduction for land-use identification. Photogramm Eng Remote Sens, 58: 423–437
Gong P, Howarth P J. 1992b. Land-use classification of SPOT HRV data using a cover-frequency method. Int J Remote Sens, 13: 1459–1471
Gong P, Liang S, Carlton E, et al. 2012. Urbanization and health in China. Lancet, 379: 843–852
Gong P, Wang J, Yu L, et al. 2013. Finer resolution observation and monitoring of global land cover: First mapping results with Landsat TM and ETM+ data. Int J Remote Sens, 34: 2607–2654
Gupta R K, Prasan T S, Krishna R, et al. 2000. Problems in upscaling of high resolution remote sensing data to coarse spatial resolution over land surface. Adv Space Res, 26: 1111–1121
Hansen M C, DeFries R S, Townshend J R G, et al. 2000. Global land cover classification at 1 km spatial resolution using a classification tree approach. Int J Remote Sens, 21: 1331–1364
Hansen M C, Potapov P V, Moore R, et al. 2013. High-resolution global maps of 21s-centrury forest cover change. Science, 342: 850–853
He H S, Ventura S J, Mladenoff D J. 2002. Effects of spatial aggregation approaches on classified satellite imagery. Int J Geogr Inf Sci, 16: 93–109
Hijmans R J, Cameron S E, Parra J L, et al. 2005. Very high resolution interpolated climate surfaces for global land areas. Int J Climatol, 25: 1965–1978
Jensen J R, Zown D C. 1999. Remote sensing of urban/suburban infrastructure and socio-economic attributes. Photogramm Eng Remote Sens, 65: 611–622
Jung M, Henkel K, Herold M, et al. 2006. Exploiting synergies of global land cover products for carbon cycle modeling. Remote Sens Environ, 101: 534–553
Kitron U, Clennon J A, Cecere M C, et al. 2006. Upscale or downscale: applications of fine scale remotely sensed data to Chagas disease in Argentina and schistosomiasis in Kenya. Geospatial Health, 1: 49–58
Kovalskyy V, Roy D P. 2013. The global availability of Landsat 5 TM and Landsat 7 ETM+ land surface observations and implications for global 30m Landsat data product generation. Remote Sens Environ, 130: 280–293
Liang L, Xu B, Chen Y L, et al. 2010. Combining spatial-temporal and phylogenetic analysis approaches for improved understanding on global H5N1 transmission. PLoS One, 5: e13575
Loveland T R, Reed B C, Brown J F, et al. 2000. Development of a global land cover characteristics database and IGBP DISCover from 1 km AVHRR data. Int J Remote Sens, 21: 1303–1330
Matthews E. 1983. Global vegetation and land use: New high resolution data bases for climate studies. J Clim Appl Meteorol, 22: 474–487
Mauser W, Schadlich S. 1998. Modelling the spatial distribution of evapotranspiration on different scales using remote sensing data. J Hydrol, 212-213: 250–267
Moody A, Woodcock C E. 1994. Scale-dependent errors in the estimation of landcover proportions—Implications for global land-cover datasets. Photogramm Eng Remote Sens, 60: 585–594
Moody A, Woodcock C E. 1995. The influence of scale and the spatial characteristics of landscapes on land-cover mapping using remote sensing. Landsc Ecol, 10: 363–379
Olson D M, Dinerstein E, Wikramanayake E D, et al. 2001. Terrestrial ecoregions of the world: A new map of life on Earth. Bioscience, 51: 933–938
Olson J S, Watts J A. 1982. Major World Ecosystem Complex Map Oak Ridge. TN: Oak Ridge National Laboratory
Quattrochi D A, Goodchild M F. 1997. Scale in Remote Sensing and GIS, 1–72. Boca Raton, FL: Lewis
Raj R, Hamm N, Kant Y. 2013. Analysis the effect of different aggregation approach on remotely sensed data. Int J Remote Sens, 34: 4900–4916
Ramirez-Villegas J, Jarvis A. 2010. Downscaling global circulation model outputs: The Delta method decision and policy analysis working paper No.1. Available: WWW document] URL: http://www.ccafs-climate.org/downloads/docs/Downscaling-WP-01.pdf [Accessed: 2 January 2013]
Sexton J O, Song, X, Feng M, et al. 2013. Global, 30-m resolution continuous fields of tree cover: Landsat-based rescaling of MODIS Vegetation Continuous Fields with lidar-based estimates of error. Int J Dig Earth, 6: 427–448
Schneider A, Friedl M A, Potere D. 2009. A new map of global urban extent from MODIS data. Environ Res Lett, 4: 044003
Schneider A, Friedl M A, Potere D. 2010. Monitoring urban areas globally using MODIS 500 m data: New methods and datasets based on urban ecoregions. Remote Sens Environ, 114: 1733–1746
Small C. 2005. A global analysis of urban reflectance. Int J Remote Sens, 95: 335–344
Sterling S, Ducharne A. 2008. Comprehensive data set on global land cover change for land surface model applications. Glob Biogeochem Cycle, 22: GB3017
Tateishi R, Uriyangqai B, Al-Bilbisi H, et al. 2011. Production of global land cover data—GLCNMO. Int J Dig Earth, 4: 22–49
Turner M G, Dale V H, Gardner, R H. 1989a. Predicting across scales: Theory development and testing. Landsc Ecol, 3: 235–252
Turner M G, O'Neill R V, Gardner R H, et al. 1989b. Effects of changing spatial scale on the analysis of landscape pattern. Landsc Ecol, 3: 153–162
Vancutsem C, Marinho E, Kayitakire F, et al. 2013. Harmonizing and combining existing land cover/land use datasets for cropland area monitoring at the African continental scale. Remote Sensing, 5: 19–41
Verburg P H, Neumann K, Nol L. 2011. Challenges in using land use and land cover data for global change studies. Glob Change Biol, 19: 974–989
Wang J, Li C, Yu L, et al. 2014. Mapping global land cover in 2001 and 2010 with spatial-temporal consistency at 250 m resolution, ISPRS-J Photogramm Remote Sens, doi: 10.1016/j.isprsjprs.2014.03.007
Wang L, Gong P, Ying Q, et al. 2010. Settlement extraction over North China Plain with Landsat and Beijing-1 data using an improved watershed segmentation algorithm. Int J Remote Sens, 31: 1411–1426
Wang L, Li C, Ying Q, et al. 2012. China's urban expansion from 1990 to 2010 determined with satellite remote sensing. Chin Sci Bull, 57: 2802–2812
Wessel P, Smith W H F. 1996. A global self-consistent, hierarchical, high-resolution shoreline database. J Geophys Res, 101: 8741–8743
Wilby R L, Wigley T M L. 1997. Downscaling general circulation model outputs: A review of methods and limitations. Prog Phys Geogr, 21: 530–548
Wilson M F, Henderson-Sellers A. 1985. A global archive of land cover and soils data for use in general circulation climate models. Int J Climatol, 5: 119–143
Woodcock C E, Strahler A H. 1987. The factor of scale in remote sensing. Remote Sens Environ. 21: 311–332

Yu L, Holden E J, Dentith M C, et al. 2012. Towards the automatic selection of optimal seam line locations when merging optical remote sensing images. Int J Remote Sens, 33: 1000–1014

Yu L, Wang J, Gong P. 2013a. Improving 30 meter global land cover map FROM-GLC with time series MODIS and auxiliary datasets: A segmentation based approach. Int J Remote Sens, 34: 5851–5867

Yu L, Wang J, Clinton N, et al. 2013b. FROM-GC: 30 m global cropland extent derived through multi-source data integration. Int J Dig Earth, 6: 521–533

Zhao S Q, Liu S, Li Z, et al. 2010. A spatial resolution threshold of land cover in estimating terrestrial carbon sequestration in four counties in Georgia and Alabama, USA. Biogeosciences, 7: 71–80

Zhong L, Gong P, Biging G S. 2012. Phenology-based crop classification algorithm and its implications on agriculture water use assessments in California's Central Valley. Photogramm Eng Remote Sens, 78: 799–819

Zhong L, Gong P, Biging G S. 2014. Efficient corn and soybean mapping with temporal extendability: A muti-year experiment using Landsat imagery. Remote Sens Environ, 140: 1–13

Zhu P, Gong D. 2014. Suitability mapping of global wetland areas and validation with remotely sensed data. Sci China Earth Sci, doi: 10.1007/s11430-014-4925-1